JOURNAL OF PROPULSION AND POWER
Vol. 25, No. 1, January–February 2009

Shroud and Ejector Augmenters for Subsonic Propulsion and Power Systems

M. J. Werle* and W. M. Presz Jr.†
FloDesign, Inc., Wilbraham, Massachusetts 01095

DOI: 10.2514/1.36042

A new, simple, and handy control-volume formulation is put forward for propellers in ejector–augmenter systems where power is either added (e.g., for propulsion) or extracted (e.g., wind/water turbines.) The formulation is first principles based, free of empiricisms, overcomes past formulation limitations, and uncovers heretofore unknown high performance potential for such systems. For shrouded props, these new control-volume based predictions are shown to agree well with both independent experimental and computational data, as well as other analytical and empirical models. Solutions generally involve simple polynomials with a single input parameter that is easily determined from the aerodynamic performance of the empty shroud. This formulation provides new correlation parameters, plus greatly simplifies design optimization studies by decoupling the shroud and ejector design effort from that of the prop design.

Nomenclature

A	=	flow cross-sectional area
a	=	coefficient
b	=	coefficient
C_D	=	disk-loss coefficient
C_P	=	power coefficient
C_{pP}	=	pressure coefficient based on velocity V_P
C_S	=	duct/shroud force coefficient
C_{TP}	=	thrust coefficient based on velocity V_P
D	=	diameter
F_S	=	duct/shroud force
F_{S1}, F_{S2}	=	duct/shroud forces
g	=	coefficient
K_t	=	thrust coefficient $= T/\rho n^2 D_p^4$
n	=	propeller rotational speed in revolutions per minute
P	=	power
P_{iH}	=	shaft horsepower
p	=	pressure
r	=	power ratio
r_S	=	ejector inlet area ratio $= A_S/A_D$
T	=	thrust
u	=	V/V_a
V	=	velocity
V_c	=	characteristic velocity
V_n	=	velocity normal to shroud
V_P	=	"power" velocity
v	=	V/V_c
z	=	coefficient
η	=	propeller efficiency
ρ	=	fluid density

Subscripts

a	=	ambient freestream conditions
D	=	properties at duct exit plane
d	=	properties in ejector duct
E	=	properties at ejector duct exit plane
m	=	maximum power state
o	=	properties at downstream outlet area
p	=	conditions at the propeller plane,
S	=	properties at ejector inlet
T	=	flow conditions for finite tunnel cross-sectional area
0	=	properties when $V_a = 0$
1, 2	=	properties fore and aft of the prop, respectively

Received 4 December 2007; revision received 18 July 2008; accepted for publication 21 July 2008. Copyright © 2008 by FloDesign Inc.. Published by the American Institute of Aeronautics and Astronautics, Inc., with permission. Copies of this paper may be made for personal or internal use, on condition that the copier pay the $10.00 per-copy fee to the Copyright Clearance Center, Inc., 222 Rosewood Drive, Danvers, MA 01923; include the code 0748-4658/09 $10.00 in correspondence with the CCC.

*Chief Scientist, 390 Main Street. Fellow AIAA.

†Emeritus Professor of Mechanical Engineering and Chief Technology Officer, Western New England College, 390 Main Street. Member AIAA.

I. Introduction

THERE has been considerable effort and discussion in the literature (see, for example, [1–8]) concerning the potential for shrouded power generators (wind and/or water turbines) such as depicted in Fig. 1 to outperform their unshrouded counterparts, most based on limited experimental and/or incomplete analytical formulations. Additionally, although ejector-based propulsion augmentation has been studied extensively for over 60 years (see [9–16] for examples), only limited attention has been given its application to subsonic/incompressible propulsors and power generators. This paper addresses both these shortfalls and extends the work of [17] to provide a new, corrected, unified and handy formulation applicable to ejector-augmented prop systems such as applicable to propulsors and/or power generators.

For ejector-based augmentation, literally hundreds, if not thousands, of papers, articles, reports, and books have discussed this problem at length (see [9–16] for a representative sampling) for configurations, such as depicted in Fig. 2, involving interactions between primary and secondary streams that are fluid dynamically independent. Two key papers on the subject are those of von Kármán ([10] and as discussed in [9], for example) and Heiser ([11]). Von Kármán introduced the simple one-dimensional momentum balance model of Fig. 2 to predict the amplification of a primary jet's thrust due to ingestion of freestream fluid into a constant area duct that exhausts to the freestream's static pressure level. All efforts since that time have employed this same basic model with its two critical assumptions/constraints: 1) independent primary and secondary streams plus 2) all the mixed flow exiting the ejector at the freestream pressure level. These both are inappropriate for low-speed/incompressible flow through prop-based systems. For these, the primary stream is but a portion of the freestream modified due to power injection or extraction. Also, the imposition of the freestream pressure at the ejector exit is a specialized case and is inappropriate

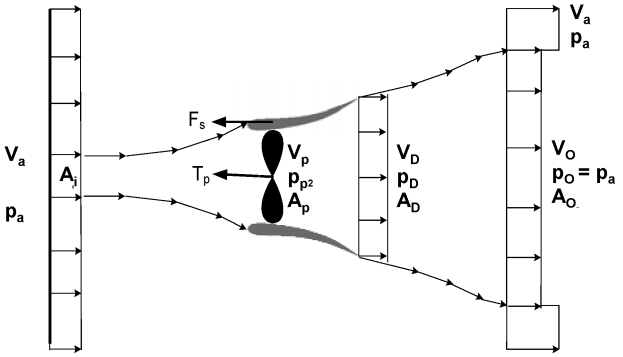

Fig. 1 Shrouded system nomenclature.

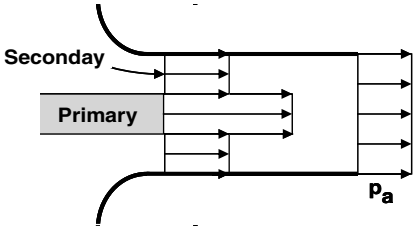

Fig. 2 Traditional ejector model.

for subsonic or incompressible ejector applications, a fact not yet accounted for in the literature.

The current study extends the shrouded prop system flow formulation of [17] to include an ejector augmenter incorporated into the shroud as depicted in Fig. 3. In this case, the entire system is strongly coupled fluid dynamically such that the ejector augmenter affects the primary flow and vice versa. Only the single stage results will be discussed herein with the multiple stage results the subject of a later paper.

The complete, unified formulation for shrouded and augmented prop systems provided here is straightforward but both new and tedious. It is therefore presented in stepwise fashion—first introducing and verifying basic concepts for the shrouded case in Sec. II and thereafter extending the formulation to the case of a one-stage ejector augmenter in Sec. III. The governing equations are first presented in a unified dimensional form, then in the nondimensional form appropriate to their application either for propulsors or power generators. These are followed by discussion of the solution methodologies, sample verifying comparisons with other solutions and data, followed by a compendium of results for study, analysis, and design guidance.

II. Shrouded Propulsors and Power Generators

A. Formulation Review and Verification

Figure 1 provides the geometry and nomenclature applied here to both propulsors and power generators. The formulation first presented in [17] employs two key elements that differentiate it from previous works: the imposition of boundary conditions infinitely far downstream (as used in the most previous propulsion but not power generation applications) combined with the explicit incorporation into the formulation of the shroud produced axial force F_S, shown in Fig. 1.

With regard to the downstream boundary condition, its use in analytical models is well known and understood for shrouded propulsors (see [9], for example) as well as for unshrouded power generators (see [18,19], for example.) Only Hansen et al. ([4,18]) and Grassmann et al. ([7]) used a closure condition far downstream in a multidimensional computational fluid dynamic (CFD) analysis of a simulated shrouded wind turbine. In the current model the pressure boundary condition is imposed at downstream infinity for a generalized one-dimensional model of shrouded systems.

For the shroud force F_S, an entirely new formulation was introduced in [17,20]. To solidify concepts, it is first useful to review the flow physics attendant to the shrouded propellers and/or blades. As discussed in [9], in the inviscid, incompressible shrouded flow depicted in Fig. 4, any axial pressure change due to the energy addition or extraction by a propeller, for example, causes the flow streamlines to expand or contract laterally, giving rise to a velocity component normal to the shroud. Because of this, the Kutta–Joukowski theorem requires an axial force F_S to occur as a result of the interaction between the normal velocity component with the ring vortex vector associated with the duct's circulation. The critical aspect of this theoretical model is that it relates the axial force on the shroud solely and directly to the energy addition or extraction at the propeller location. From this concept and dimensional analysis considerations, the formulation of [17,20] therefore took the shroud force to be proportional to the prop induced force through a newly defined axial force coefficient C_s, such that

$$F_S = A_p(p_{p2} - p_{p1})C_S \tag{1}$$

Equation (1) represents a significant departure from traditional approaches that tend to relate all forces on bodies immersed in fluids linearly to the dynamic pressure of the freestream flow. According to inviscid flow theory, this is inappropriate here because the controlling mechanism is the axial pressure change, not the freestream dynamic pressure.

A momentum, mass, and energy balance is then applied to the flow structure and the cut of Fig. 5 for an arbitrary but finite wind-tunnel–like flow cross-sectional area, A_T. The assumptions applied are as follows:

1) The flow is that of an inviscid incompressible fluid moving through a conduit of cross-sectional area, A_T.

2) The fluid has a uniform pressure and velocity at the conduit's upstream-infinity entrance.

3) The fluid exits the conduit at downstream infinity with a uniform pressure p_o and a slipstream exists between the mainstream flow exiting at V_T and the fluid exiting at velocity V_o that passed through the prop.

4) The cuts around the prop and shroud shrink to their respective surfaces.

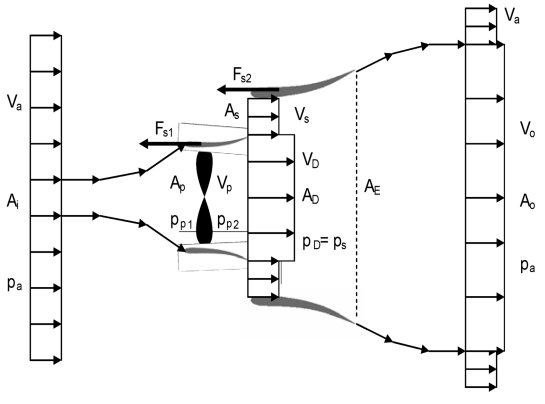

Fig. 3 Ejector–augmenter nomenclature.

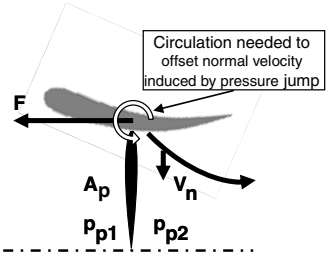

Fig. 4 Axial force source.

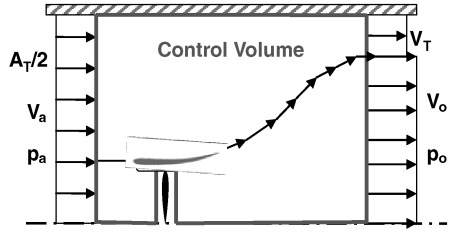

Fig. 5 Shroud control volume.

5) The force on the prop equals the pressure jump acting on the prop area A_p and the sum of the pressure forces acting on the shroud are given by Eq. (2).

The resulting equations form a closed set solvable for any cross-sectional area A_T. For current purposes, attention is focused on the case of $A_T \gg A_p$, resulting in a simple set of algebraic relations applicable equally to shrouded propulsors and power generators, as will be discussed in respective detail next. For this case, Eq. (1) can be rewritten using Bernoulli's equation as

$$F_S = 1/2\left[\rho A_p\left(V_o^2 - V_a^2\right)\right]C_S \tag{2}$$

B. Shrouded Propulsors

For this case, one has a choice as to the principle independent variable to be applied depending on which is most appropriate to the situation. As in [17,20], here the power through the propeller to the flowfield is used to allow a detailed assessment of the thrust potential at fixed input power levels. For this case, Werle and Presz in [17,20] nondimensionalized the governing equations using the following definitions:

$$V_c \equiv V_P/(1 + C_S)^{1/3} \tag{3}$$

$$V_P \equiv (4P/\rho A_p)^{1/3} \tag{4}$$

$$v_o \equiv V_o/V_c, \qquad v_p \equiv V_p/V_c, \qquad v_a \equiv V_a/V_c \tag{5}$$

Note that the power velocity V_P of Eq. (4) is closely related to the disk loading coefficient used by others, for example, [9]. The exact solution to the governing equations is then given as

$$v_o = (1/2)^{1/3}\left[1 + 16/27v_a^3 + \sqrt{1 - 32/27v_a^3}\right]^{1/3} + (1/2)^{1/3}\left[1 + 16/27v_a^3 - \sqrt{1 - 32/27v_a^3}\right]^{1/3} - v_a/3 \tag{6}$$

which can be approximated using a Taylor series expansion to write that

$$v_o \approx 1 - 1/3v_a + 4/9v_a^2 \tag{7}$$

These in turn were used to calculate the shrouded systems total thrust in terms of a new thrust coefficient defined as

$$C_{TP} \equiv \frac{T}{(1/2)\rho A_p V_P^2} = \frac{(1 + C_S)^{1/3}}{(v_a + v_o)} \approx \frac{(1 + C_S)^{1/3}}{[1 + \frac{2}{3}v_a + \frac{4}{9}v_a^2]} \tag{8}$$

As noted in [17,20], the bare prop case for static flight is recovered from Eq. (8) when $C_S = 0$, as but one of an infinite family of cases, all of which are well represented by the approximate version of Eq. (8) for both static and forward flight conditions. Also note that the current formulation and results apply for both hover and forward flight conditions without constraints and/or need of any special treatment as V_a goes to zero. This formulation was further simplified to show that

$$C_{TP0} \equiv (C_{TP})_{V_a=0} = (1 + C_S)^{1/3} = \left(\frac{V_p}{V_a}\right)_{P=0} \tag{9a}$$

or

$$C_{TP0} \approx \left(2\frac{A_D}{A_p}\right)^{1/3} - \frac{A_D}{A_p}C_{pPD} \tag{9b}$$

where C_{pPD} is the pressure coefficient, based on V_P, at the shroud exit plane, A_D. Most importantly, Eq. (9) shows that C_S is directly related to C_{TP} at $V_a = 0$ when $P > O$ as well as V_p/V_a at $P = 0$ when $V_a > 0$. Additionally, Eq. (9) shows that the shroud diffusion and exit pressure levels are interdependent and cannot be considered separately as has been done in many previous studies.

In [17,20] and the current work, the shroud diffusion level given by A_D/A_p is kept at or below 1.3, because higher levels are known to generate unacceptable viscous losses. Nonetheless, using Eqs. (8) and (9), Werle and Presz [17,20] showed that for this static velocity case 1) thrust increases of nearly 80% above the bare propeller level are potentially attainable with moderate diffusion and exit plane suction pressures, and 2) the handy approximations of Eqs. (8) and (9) give a good representation for both the bare and the entire family of shrouded prop cases for virtually all forward velocity levels.

Combining Eqs. (8) and (9) also provides handy and accurate relations for all unshrouded and shrouded props at any power and forward velocity level as

$$\frac{C_{TP}}{C_{TP0}} = \frac{T}{T_0} \approx \frac{1}{1 + \frac{2}{3}v_a + \frac{4}{9}v_a^2} \tag{10a}$$

$$\frac{C_{TP}}{C_{TP0}} = \frac{T}{T_0} \approx \frac{1}{1 + \frac{2}{3}C_{TP0}\frac{V_a}{V_P} + \frac{4}{9}C_{TP0}^2\frac{V_a^2}{V_P^2}} \tag{10b}$$

Because the formulation and results presented in [17,20] and above are new and different, it is appropriate to provide evidence of their validity through comparisons with experimental data and other analytical models. Figures 6 and 7 provide comparisons with the experimental and computational data of Van Manen and Superine in [21] and Bulten and van Esch ([22]) along with the analytical results of McCormick ([9]), who used the circulation based approximate model of Weissinger ([23]).

Van Manen and Superine ([21]) provide an extensive database for shrouded props as used in ship propulsors. Variations in shroud geometries were studied over a wide range of prop advance ratios and loadings for a fixed rotor speed. The measured thrust levels for two of the shrouds, designated N7 and N18, are provided in Figs. 6a and 6b in two forms. Results for two additional geometries were also provided in [21], but were found to fall between those presented in Fig. 6 and thus added little to the verification process. Also shown are the experimental and computational (CFD) results of Bulten and van Esch as presented in [22]. For all the cases shown, the original data were presented as families of smooth continuous curves, not discrete data points. Thus there exists some uncertainty as to the range of experimental variation in the measured results. For current purposes, the data have been marked here with discrete symbols at each advance ratio for identification purposes only.

Converting the data of [21,22] to the current variables requires determination of the power being injected into the fluid by the prop. Although it is known to be some percentage of the measured prop shaft torque multiplied by the rotor speed, the precise value was not explicitly stated in either [21] or [22]. Thus, for present purposes, the prop efficiency factor was determined two ways. The first of these employed a separate analysis of the Ref. [21] data set indicating prop efficiency values ranging from 0.71 to 0.85 depending on the nozzle and advance ratio. These were determined by making use of the approximation recommended by Van Manen and Superine ([21]) for estimating the velocity at the prop station, which was not measured directly but rather inferred from separate tests. This approximation, originally due to Froude, assumes that the prop advance ratio in the

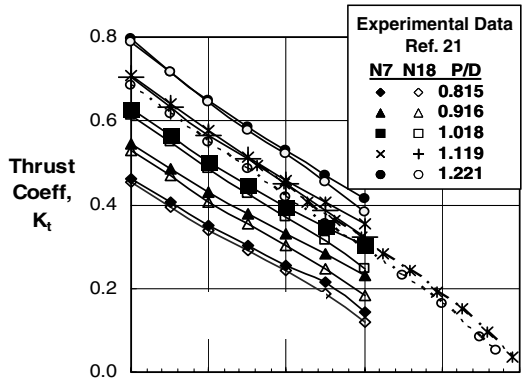

a) Thrust data

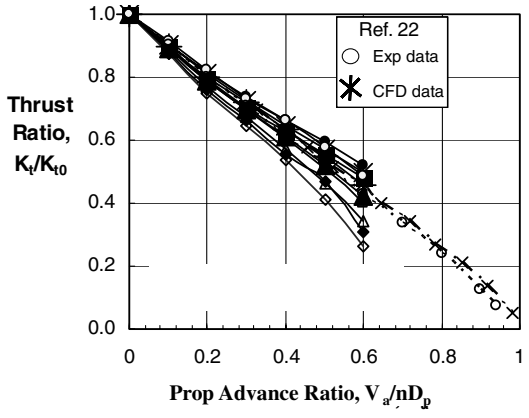

b) Thrust ratio data

Fig. 6 Shrouded propulsor data.

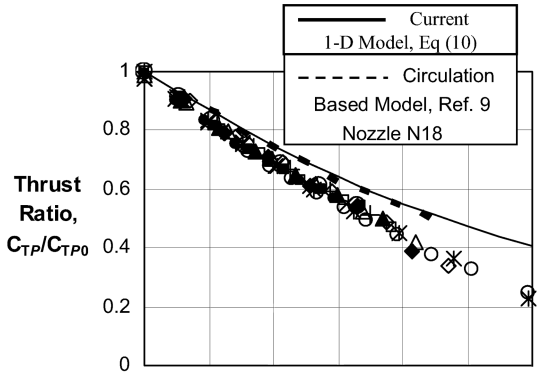

a) Inferred efficiencies

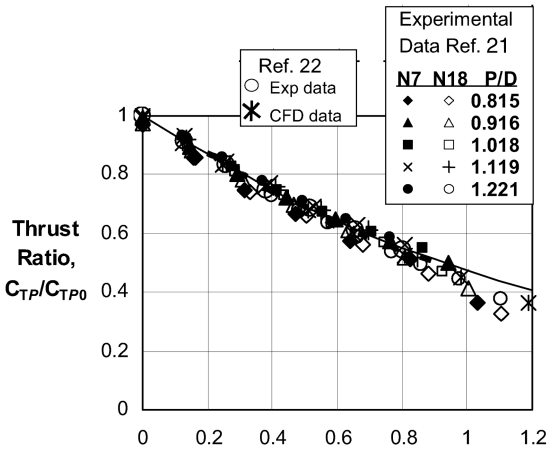

b) Estimated efficiencies = 0.65

Fig. 7 Shrouded propulsor models and data correlations.

shroud is the same as that in a cylinder at the same level of the nondimensionalized thrust. With this and the measured nozzle and prop thrust plus torque data, one can estimate prop efficiency and thereafter the parameters of the current formulation. The resulting C_S values were 0.76 and 1.0 for the N7 and N18 nozzles, respectively. For the results shown from [22], the experimental data were found to have $C_S = 0.57$ and the CFD data $C_S = 0.37$. As shown in Fig. 7a, use of these prop efficiency estimates and the parameters of Eq. (10), quite remarkably, cause all the data presented in Fig. 6 to collapse to a single set. Further, the results are seen to necessarily lie below but closely track the current maximum thrust prediction over the full range of forward velocities, thus providing a strong endorsement of the current theoretical formulation and the utility of the correlation/scaling parameters it provides.

Because a level of uncertainty exists in the method described previously for calculating prop efficiencies due to the fact that the prop's radial flow distributions between the two cases used in the Froude methodology would likely differ, a second method has also been used here for estimating the prop efficiency. For this a prop efficiency value that best aligned the data with the predictions was chosen; in this case a value of 0.65 applied to all the data. This level of prop efficiency is seen in Fig. 7b to shift the entire data set virtually on top of the current model predictions.

Also shown in Fig. 7 are the analytical predictions provided by McCormick ([9]) for the N18 configuration of [21]. These were obtained using the somewhat tedious scheme developed by Weissinger ([23]), wherein the prop's influence on the circulation about the shroud is approximated by a set of elaborate calculations involving tables and charts of tabulated results. To include the results of [9] in Fig. 7 requires knowledge of the solution at $V_a = 0$, which was not provided. For current purposes, it was assumed that Eq. (10) was valid between $V_a = 0$ and the lowest value of V_a provided by [9], which in the current terms was found to be at $V_a/V_c = 0.2$. This defacto guarantees that McCormick's curve intersects the current solution at that point. Quite pleasingly, it is seen that the two results are virtually the same for all velocities thereafter, further highlighting and verifying the general utility of the current formulation and its attendant correlation parameters.

Finally, in closing this discussion relative to verifying the shrouded prop's formulation, attention is now given to the current model's ability to predict the static thrust level C_{TP0}, defined in Eqs. (8) and (9). These have been used for comparisons with the data and empirical predictions of [24,25], which were presented in terms of a thrust-to-power ratio and diameter/disk-loading parameter for a very wide range of configurations, from air cushion machines to helicopters. Marc de Piolenc and Wright [24] introduce a shaft input power in horsepower P_{iH}, which is related to the power P through the prop efficiency factor by the relation:

$$P \equiv \eta 550 P_{\mathrm{iH}} \tag{11}$$

Marc de Piolenc and Wright [24] provided the experimental data in graphical form using the two parametric groupings:

$$T/P_{\mathrm{iH}},\ \sqrt{D_p 1000/P_{\mathrm{iH}}} \tag{12}$$

which allow one to use Eqs. (8) and (9) to write for air that

$$T/P_{\mathrm{iH}} = 0.85(1 + C_S)^{1/3}[D_p\sqrt{1000/P_{\mathrm{iH}}}]^{2/3} \tag{13}$$

where use has been made of a prop efficiency ratio of 0.75 as proposed in [24]. For the bare prop case, $C_S = 0$ and the prediction of Eq. (13) is found to reproduce those empirical relations provided in [24,25] plus compare well with the data as shown in Fig. 8. Additionally, for a shrouded prop with an area ratio of 1 and zero exit pressure coefficient, Eq. (9) gives $C_S = 1$ and Eq. (13) is found to again exactly reproduce the correlation expressions of [24,25] plus, as seen in Fig. 8, to well represent the shrouded data and trends. It is also found that for a shroud area ratio of 2, the prediction of Eq. (13) again reproduces the empirical expression of [25]. As such, these results plus those of Fig. 7 verify the current formulation's ability to

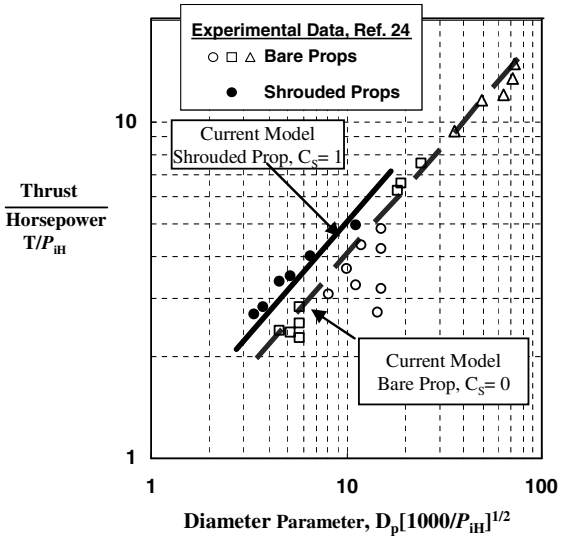

Fig. 8 Bare and shrouded prop static thrust data.

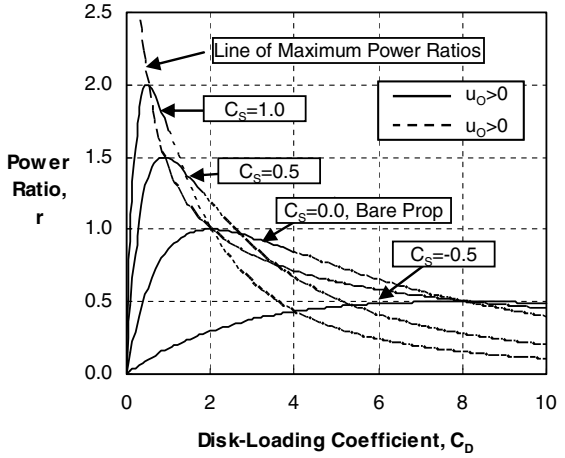

Fig. 9 Disk-loading influence on shrouded power generator.

represent the flow attendant to bare and shrouded prop systems at any forward velocity.

C. Shrouded Power Generators

For this case, it is appropriate to nondimensionalize the governing equations, as in [17,20], using the freestream velocity V_a to write that

$$u_o \equiv V_o/V_a, \qquad u_p \equiv V_p/V_a \tag{14}$$

leading to the simple relation for the power extracted as

$$C_P \equiv \frac{-P}{(1/2)\rho A_p V_a^3} = (1 + C_S)(u_o + 1)\left(1 - u_o^2\right)/2 \tag{15}$$

Two methods have been employed in the literature and in [17,20] to determine the power extractable, the maximum power approach, and the disk-loss approach. Both have equal but different utility and will be applied here. For the maximum power approach, the derivative of C_P with respect to u_o is set to zero to yield

$$C_{Pm} = \frac{16}{27}[1 + C_S] \tag{16}$$

As discussed in [17,20], Eq. (16) is the long sought but heretofore undiscovered, correct generalization to shrouded power generators of Betz's bare prop limit of the power extractable from a stream (see [18,19], for example), which is recovered here as but one of an infinite family of solutions for the case when there is no shroud force, that is, $C_S = 0$. Most importantly, it is seen that the maximum power level is completely and uniquely established by a single parameter, the shroud axial force coefficient C_S, which, as for the shrouded propulsor, is easily determined from the velocity ratio V_p/V_a at $P = 0$.

The validity and utility of the current formulation was demonstrated in [17,20] through comparison with the CFD results of Hansen et al. ([4]) over a range of the power extraction levels for flow through an actuator disk simulating a pressure drop across a power generator. Excellent comparisons were shown between the current model and the more complete viscous CFD analysis for both an unshrouded case as well as an aerodynamically contoured shrouded case with an aggressive exit area ratio, $A_D/A_p = 1.86$.

References [17,20] and others (see Refs. [1,2] for example), uses the disc-loss coefficient, C_D, to write the total pressure change across the plane of the prop (the disc) as

$$C_D \equiv \frac{p_{p2} - p_{p1}}{1/2\rho V_p^2} \tag{17}$$

which leads to

$$r \equiv \frac{27}{16}C_P = \frac{27}{2}\left(\frac{(1 + C_S)/2}{1 + (1 + C_S)^2 C_D/4}\right)^3 C_D \tag{18}$$

Results from using Eq. (18) are shown in Fig. 9 for C_S varying from −0.5 to 1.0, showing the classic shape observed by Igar ([1,2]) and others. Also included is the loci of points of maximum power extraction predicted by Eq. (16). It is important to note that when $C_D = 2C_{D\max}$, the downstream outlet velocity u_o will pass through zero, which from the continuity equation requires that the downstream outlet area becomes infinite, signaling the limit of the current formulation's validity. Thus the power ratio results shown in Fig. 9 are only valid up to the start of the dashed portions of the curves. At these limit disk-loading levels, the disk is extracting so much energy from the flow that its velocity far downstream is vanishingly small and further loading would result in massive stall of the system and recirculation of the flow aft of the turbine.

Figure 9 indicates that for nearly all values of disk loss C_D, shrouds with $C_S < 0$ (i.e., $u_{p0} < 1$) produce less power than the bare prop, mainly because the shroud is acting to slow down the flow as it approaches the prop station. For $C_S > 0$ (i.e., $u_{p0} > 1$) the flow is sped up and it is seen in Fig. 9 that 1) the maximum power extraction limits dramatically exceed that of the bare prop, and 2) they consistently do so at lower level C_D. Thus, it must be appreciated that achieving such high levels of power extraction indicated will require carefully designed systems to assure the C_S and C_D levels are correctly chosen so as to avoid rapid performance drop-off on either side of the peak design levels as well as the massive stall lurking at higher C_D levels.

With Eqs. (17) and (18), comparisons can now be conducted with controlled shrouded power generator experimental studies, which have largely been conducted using screens to generate the disk-loss terms. Igar ([1,2]) conducted numerous such studies, virtually all of which show levels of maximum power above the Betz limit as high as $r_m = u_{p0} = 3.5$, corresponding to $C_S = 2.5$. Of all the data, one set presented in [1] contains enough information to apply the current model. It is that of a shroud formed by a NACA 4412 airfoil and is designated by Igar ([1]) as the C_i shroud. For this case, both the values of power extracted r and throat velocity $V_p/V_a = u_p$ are given for a range of C_D values >0, with some of the data measured in a small wind tunnel and some in a large wind tunnel. With the range of throat velocity values given, its value u_{p0} for P or $C_D = 0$ can be determined and thus the shroud's axial force coefficient C_S from Eq. (4) with $V_a = V_o$. This gives a value of $u_{p0} = 1.7$ and thus a value of $C_S = 0.7$. With this, Eq. (18) was used to calculate the values of r presented in Fig. 10. It is seen that very good agreement with the experimental measurements is achieved, including the level and position of the maximum power extracted, adding further evidence of the validity and utility of the current formulation.

Finally, a universal correlation for all wind turbine shrouds can be written by combining Eqs. (14), (15), and (18) to write that

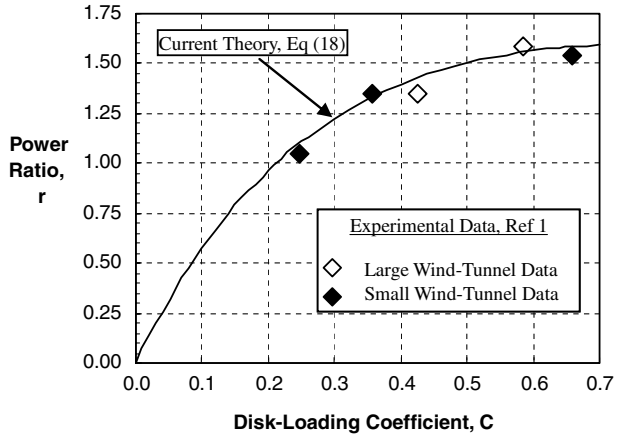

Fig. 10 Power generator experimental comparisons.

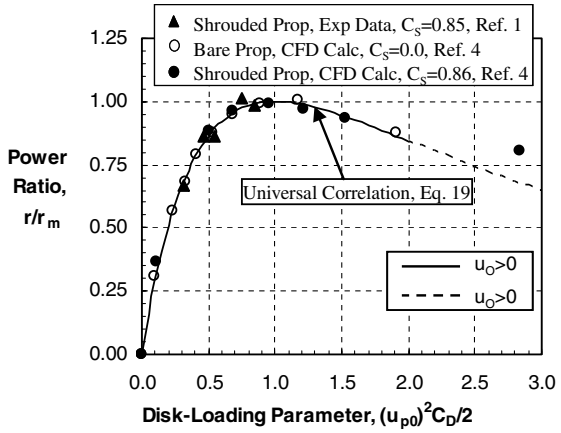

Fig. 11 Power generator power correlation.

$$r/r_m = \frac{27\left(u_{p0}^2 C_D/2\right)}{\left[2+\left(u_{p0}^2 C_D/2\right)\right]^3} \tag{19}$$

This simple relation defines the power that can be extracted by any unshrouded or shrouded system for any disk-loading value of C_D. As shown by the solid line in Fig. 11, the peak value of $r/r_m = 1$ always occurs at $u_{p0}^2 C_D/2 = 1$ and all systems stall at $u_{p0}^2 C_D/2 = 2$. Also shown in Fig. 11 are the CFD results of [4] and experimental data from [1] for which the correlation values for u_{p0} (or C_S) and r_m were established from the data provided. Both the experimental and CFD cases had approximately the same C_S value near 0.85. As seen in Fig. 11 the correlation parameters collapse all the data to the single curve of Eq. (19) except the one point from the CFD calculations of [4] at a value of $u_{p0}^2 C_D/2 = 2.83$. Because this is in the zone where system stall, backflow, and/or ballooning of the prop wake is anticipated it is reasonable to assume the CFD results are tainted and can be ignored.

III. One-Stage Ejector Augmenters

A. One-Stage Ejector Formulation

To extend the shrouded flow formulation of Sec. II to that of the ejector augmenter depicted in Fig. 3, it is first necessary to take note that the ejector duct as depicted in Fig. 12 always gives rise to a pressure increase caused by the mixing of the primary and secondary streams.

This can be shown by applying a one-dimensional momentum balance to the constant area mixing region of Fig. 12 to find that

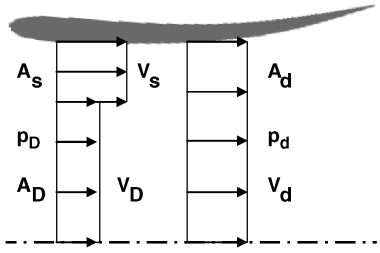

Fig. 12 Ejector mixing model.

$$p_d - p_S = \rho \frac{A_S A_D}{(A_S + A_D)^2}[V_D - V_S]^2 \tag{20}$$

Thus for a shrouded prop plus ejector, the total axial force induced on the fluid is found to have two components: that due to the pressure change across the prop discussed in Sec. II plus that due to the pressure increase (energy loss) in the ejector duct.

With Eq. (20), and following the logic of [17,20] as well as Sec. II, the force on the two shroud elements is again related to the axial pressure forces through the shroud axial force coefficient C_S as

$$F_S \equiv F_{S1} + F_{S2} = \{A_p(p_{p2} - p_{p1}) + A_d(p_d - p_s)\}C_S \tag{21}$$

and

$$A_d = A_D + A_S \tag{22}$$

Note should be taken of the fact that in Eq. (21) the definition of C_S has been generalized to include the axial force component induced by the pressure rise in the ejector duct. Although this differs in detail with that of Eq. (1) for the nonejector case, it was found that it still produced the result that $C_S = u_{p0} - 1$. Thus, at this time, there seems no apparent reason to differentiate C_S for the two cases.

As for the shrouded case, an overall momentum, mass, and energy balance can than be applied to the flow structure and the cut of Fig. 13 for a finite cross-sectional area A_T, employing the same assumptions applied earlier relative to Fig. 5 for the simple shrouded case to yield

$$F_S = \left\{\frac{1}{2}\rho A_p\left(V_D^2 - V_S^2\right) + \rho A_D(V_D - V_S)^2 \frac{r_S}{1+r_S}\right\}C_S \tag{23}$$

where r_S is the ratio of the ejector shroud inlet area A_S, to the primary shroud diameter A_D:

$$aV_D^2 - bV_S^2 - 2r_S C_S V_S V_D = (1+r_S)(V_D + r_S V_S)(V_o - V_a) \tag{24}$$

where

$$a \equiv 1/2A_p/A_D(1+C_S)(1+r_S) + r_S C_S \tag{25}$$

and

$$b \equiv 1/2A_p/A_D(1+C_S)(1+r_S) - r_S C_S \tag{26}$$

The power introduced or extracted can be related to the primary and secondary stream velocities as

$$P = 1/2\rho A_D V_D\left(V_D^2 - V_S^2\right) \tag{27}$$

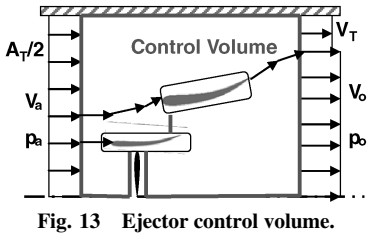

Fig. 13 Ejector control volume.

To complete the formulation, flow through the ejector duct of Fig. 12 can be related to the downstream conditions using Bernoulli's and the continuity equations to write

$$(V_S + r_S V_D)^2 = (1 + r_S)^2\left(V_D^2 + V_a^2 - V_o^2\right) \tag{28}$$

Equations (24–28) apply equally to either thrust generation due to positive power input or power extraction via a power generator, each of which is discussed in detail next.

B. One-Stage Propulsor Augmenter

The governing equations for a single stage ejector as depicted in Fig. 3 are first nondimensionalized as in Sec. II.B using the characteristic velocity V_c of Eqs. (3–5) to write

$$av_D^2 - bv_S^2 - 2r_S C_S v_S v_D = (1 + r_S)(v_D + r_S v_S)(v_o - v_a) \tag{29}$$

$$(v_S + r_S v_D)^2 = (1 + r_S)^2\left(v_D^2 + v_a^2 - v_o^2\right) \tag{30}$$

$$v_D\left(v_D^2 - v_S^2\right) = 1/2(1 + C_S)A_p/A_D \tag{31}$$

For given values of $C_s, A_E/A_d, A_D/A_p, A_E/A_p$, and v_a, Eqs. (29–31) form a closed set and can be solved iteratively, with one such scheme provided in [20]. These solutions give v_D, v_S, and v_o which are than used to calculate the output parameters of interest as follows:

Total thrust:

$$C_{TP} \equiv \frac{T}{1/2\rho A_p V_P^2} = 2\frac{A_D}{A_p}(v_D + r_S v_S)\frac{v_o - v_a}{(1 + C_S)^{2/3}} \tag{32}$$

Prop thrust:

$$C_{TP_p} \equiv \frac{T_p}{1/2\rho A_p V_P^2} = \frac{v_D^2 - v_S^2}{(1 + C_S)^{2/3}} \tag{33}$$

Exit plane pressure:

$$C_{pPE} \equiv \frac{p_E - p_a}{1/2\rho V_P^2} = \frac{v_o^2 - [(A_d/A_E)(v_D + r_S v_S)/(1 + r_S)]^2}{(1 + C_S)^{2/3}} \tag{34}$$

The results of a series of calculations for values of C_s from 1 to 3, ejector–augmenter area ratios from 1 to 5 and $V_a = 0$ are shown in Fig. 14. Because it can be shown that ejector–augmenter configurations with $C_S < 1$ do not have sufficient suction at the ejector port when r_S is small for flow to enter the ejector, they are not considered further here. Note also that due to simple geometry constraints, for the 30% diffusion cases considered here, $r_S = 0$ at $A_E/A_p = 1.3$, and thus no results are shown for values less than this value. Also, all the cases shown in Fig. 14 for $A_E/A_P = 1$ (i.e., a shrouded prop with no ejector) reproduce the shrouded propeller results provided in [17] for the same range of C_S.

It is enlightening to first consider in detail the case of $C_S = 1$ and zero diffusion, where it is noted in Fig. 14a that the exit plane pressure coefficient is exactly zero for all ejector sizes, A_E/A_p. This case is then seen to be the current equivalent of the traditionally provided solution wherein the pressure at the exit is imposed at the freestream level, that is, a pressure coefficient of zero. Whereas Fig. 14b shows that for this case the ejector can provide thrust augmentation levels of 25–70%, most importantly, it is observed that higher values of C_S introduce an entirely new family of ejector solutions with significantly higher, double or more, thrust augmentation levels over the bare propeller cases for the same input power. Note also, Fig. 14a indicates that the exit pressure level is only minimally influenced by the shrouds exit area diffusion level, whereas Fig. 14b indicates a loss in augmentation for these cases.

Figure 14c shows another major benefit of the ejector augmenter —its shifting of the bulk of the thrust loading from the prop to the shroud, that is, from the rotating to the static structure of the system. It is seen in Fig. 14 that the potential exists for moving 70 to 80% of the loading to the shroud system. The system then is capable of producing more thrust at lower power levels through a structurally more robust configuration.

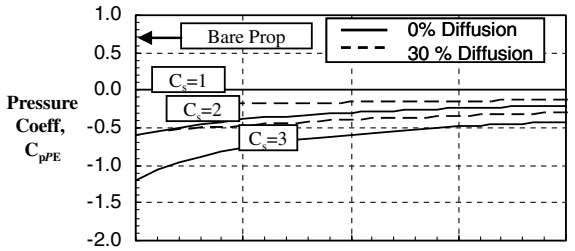

a) Exit plane pressure

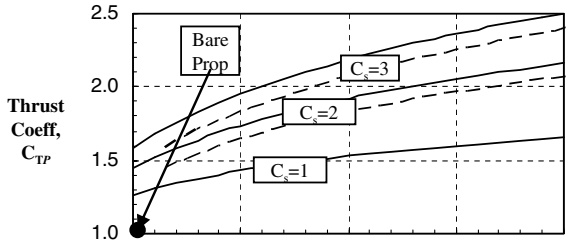

b) Total thrust augmentation

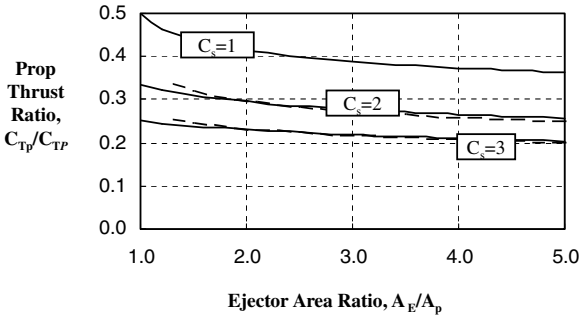

c) Prop thrust ratio

Fig. 14 Propulsor augmenter static performance.

Werle and Presz [20] provide further results including the pressure levels at both the shroud exit plane A_D and at the prop face, the point of lowest pressure in the system. There it is shown that the suction levels are very sensitive to the shroud's aerodynamics (i.e., C_S) and are further amplified when downstream diffusion is present. The primary duct exit (or ejector inlet) pressure levels were found to be less sensitive to the C_S and diffusion levels. Also provided in [20] were the downstream outlet flow areas attendant to the system. These results indicate a dramatic increase (by a factor of 10 or 20) of flow area as both C_S and the ejector area ratio A_E/A_p increase, implying that wind-tunnel testing of such configurations must take care to assure wall interference effects are kept to a minimum.

Finally, in Fig. 15 the influence of forward flight velocity on the ejector system's performance is shown for a bare prop, a shrouded prop with $C_S = 3$, and an ejector augmenter with $C_S = 3$ and $A_E/A_p = 3$. Although in Fig. 15a all cases show the expected decline with forward velocity, the ejector augmenter is seen to add significant thrust augmentation well above the bare and shrouded prop equivalents, even at relatively high forward flight speeds. Figure 15b displays the same results but in terms of the propeller efficiency levels ([9,26], for example). Although the ejector augmenter is seen to always have efficiencies above those of the bare and even shrouded prop, most notable is the large gain at lower velocities and/or higher disk-loading levels. At lower velocities with higher disk loading, prop efficiency gains of over 100% over that for a bare prop are seen to be possible.

C. One-Stage Power Generator Results

As for the shrouded case of Sec. II.C, the governing equations for the one-stage ejector depicted in Fig. 3 are nondimensionalized using

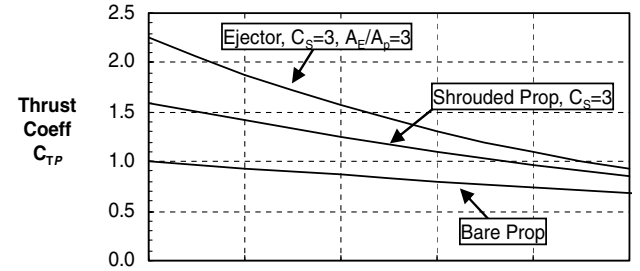

a) Thrust augmentation

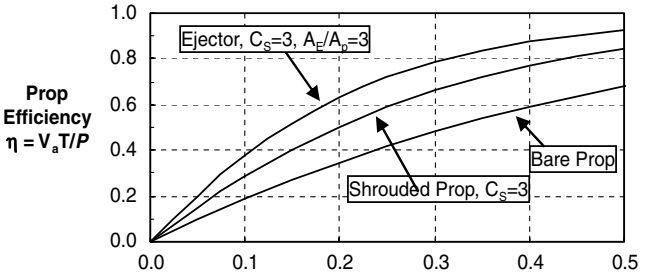

b) Prop efficiency

Fig. 15 Propulsor augmenter forward flight influence.

the definitions of Eq. (20) plus two additional ones given as

$$u_D \equiv V_D/V_a, \qquad u_S \equiv V_S/V_a \tag{35}$$

Equations (24–28) become

$$au_D^2 - bu_S^2 - 2r_S C_S u_S u_D = (1 + r_S)(u_D + r_S u_S)(u_o - 1) \tag{36}$$

$$(u_S + r_S u_D)^2 = (1 + r_S)^2\left(u_D^2 + 1 - u_o^2\right) \tag{37}$$

$$C_P = u_D\left(u_S^2 - u_D^2\right)\frac{A_D}{A_p} \tag{38}$$

As for the shrouded case of Sec. II.C, two solution methodologies have been employed here, the maximum-power approach and the disk-loss approach.

Following Sec. II.C, the maximum power extractable is determined by setting to zero the derivative of the power [Eq. (38)] with respect to the appropriate variable, in this case u_D. As shown in [20] this leads to three coupled quadratic relations that can be solved iteratively for the velocities and thus maximum power extractable from the flow. Results of the calculations are given in Fig. 16, in terms of r_m, the ratio of the maximum power available to that of its bare prop equivalent for C_S values from 0 (the bare prop) to 1, for

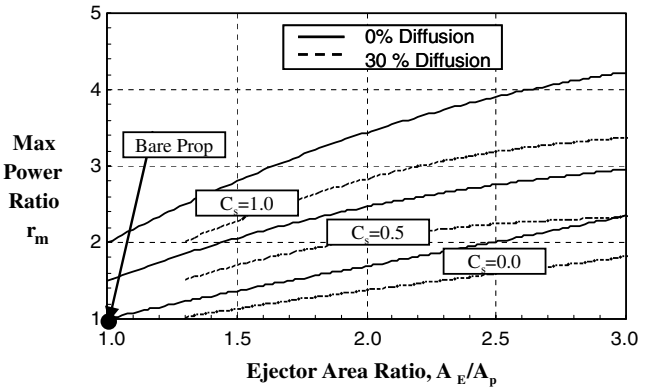

Fig. 16 Power generator augmentation limit.

which $u_{p0} = 2$. Although higher values of C_S are implied by the data of [1,2], the current range was limited for direct comparisons with the shrouded prop data of Figs. 10 and 11. As with the propulsor cases discussed in Sec. III.B above, values shown for no ejector ($A_E/A_p = 1$) reproduce the shrouded power generator results provided in [17,20] and Sec. III.C above. Figure 16 also shows that with ejector area ratios, $A_E/A_p > 1$, the ejector augmenter is capable of delivering significant levels of power augmentation, by factors of 2 and more, above that of its bare and shrouded counterparts. The influence of duct diffusion is seen to effectively be a shift in all the results to the right by the diffusion level, 0.3, which can also be viewed as a lowering of the maximum-power limit for a given ejector area ratio.

As for the propulsion case, Werle and Presz [20] also showed that the downstream outlet flow area A_o grows significantly with ejector size, and thus care has to be taken in wind-tunnel testing of such configurations to minimize wall interference effects. It also indicated a less sensitive, but still significant, growth of the upstream capture area A_i/A_p and the velocity at the prop station V_p/V_a, indicating a doubling at $C_S = 1$, over the bare prop equivalent case. Again, this would need careful consideration for wind-tunnel testing of such systems.

Turning attention now to the disk-loss method for solving Eqs. (35–38), C_D, as defined in Eq. (17), is again introduced. As shown in [20] the solution provides an algebraic relation for the maximum power extractable for any level of C_D, C_S, A_D/A_p, and ejector area ratio A_E/A_p as

$$r = \frac{27C_D}{2}\left[\frac{(A_D/A_p)(1 + r_S)(1 + gr_S)z}{(1 + gr_S)^2(1 + g + 2r_S) + (g - 1)z^2}\right]^3 \tag{39}$$

where

$$g \equiv \sqrt{1 + C_D\left(\frac{A_D}{A_p}\right)^2} \tag{40}$$

$$z \equiv \frac{1}{2}(g + 1)(1 + r_S)(1 + C_S)\frac{A_p}{A_D} - (g - 1)r_S C_S \tag{41}$$

Equation (39) reduces exactly to Eq. (11) at $r_S = 0$, that is, $A_E/A_p = 1$.

Figure 17 uses Eq. (39) to present the power augmentation predictions for all unshrouded ($C_S = 0$, $A_E/A_p = 1$) and shrouded

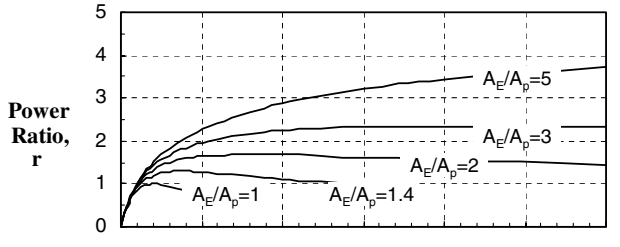

a) C_s=0

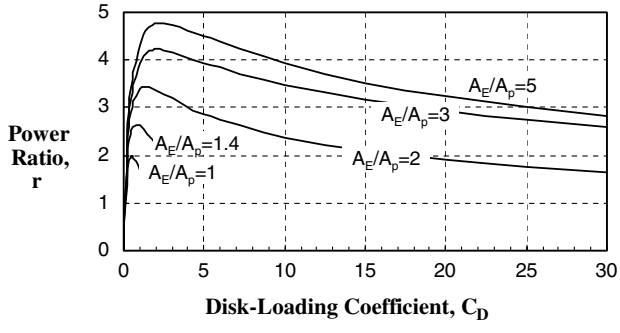

b) C_S=1

Fig. 17 Disk-loading influence on power augmentation.

props ($C_S = 1, A_E/A_p = 1$) as well as for ejector area ratios, A_E/A_p up to 5, which are the ejector equivalent of the shrouded power generator results given in Fig. 16. Note the dramatic performance improvement opportunities indicated, with power augmentation ratios as high as 4 or more shown.

Two additional important points are also immediately evident. First, Fig. 17 shows that the ejector delays the onset of reverse flow/stall over the unshrouded and shrouded equivalent, that is, $A_E/A_p = 1$. This is apparently due to the added energy brought in through the ejector ports and subsequently mixed into the core flow that passed through the prop. For the range of C_S shown, it was found that u_o was never below zero for A_E/A_p equal to or greater than 2.

The second noteworthy point is, as shown in Fig. 17, the ejector tends to flatten out the power extraction performance curves over wide ranges of C_D. This is taken as an indication that the ejector power generation system will be less sensitive to off-design effects, that is, when the velocity at the prop is not at the level it was aerodynamically designed for, the loss in performance will be much less than encountered for the shrouded or unshrouded cases. This is believed to be one of the most valuable attributes of the ejector-based power generator.

IV. Conclusions

As simple as the previous formulation is, it is hard to overstate the importance of its implications or its utility for shrouded and/or ejector-augmented prop systems. Three key critical milestones were achieved as follows:

1) A new formulation for ejector systems: A new, unified, first principals-based, empiricism-free formulation for unshrouded and shrouded prop systems with or without ejectors has been formulated and solved in terms of simple polynomials. This control volume/actuator disk model introduced three new and necessary elements:

a) Shroud forces proportional to axial prop and ejector mixing-induced pressure changes consistent with the Kutta–Joukowski theorem.

b) A coupling of the ejector's primary flow through the prop to that of the freestream secondary flow entering through the ejector shroud inlets.

c) Explicit imposition of the freestream pressure at downstream infinity instead of its traditional application at the ejector exit plane.

Taken together, these result in a fully coupled system appropriate for inviscid incompressible and/or low-speed flows. These are applicable for both hover and forward flight conditions without constraints and/or need of any special treatment as V_a goes to zero, as sometimes required by other analytical models.

2) The verification of the formulation: An extensive verification was presented of the formulation for shrouded power injecting or extracting rotor systems through comparisons with experimental data and CFD solutions, plus other appropriate analytical and empirical models.

3) The development of a compendium of new and promising solutions: The predictions resulting from the formulation have uncovered numerous heretofore unknown positive aspects of prop-based systems:

a) An infinite and continuous family of solutions dependent solely on a single input parameter, the shroud coefficient C_S, which itself can be very easily determined directly from the freestream induced velocity at the prop station when no prop is present.

b) Design and optimization studies being able to take advantage of a handy decoupling of the shroud design effort from the prop system design.

c) The heretofore unknown potential for, and pathway to, very high performance levels of thrust production and/or power extraction, as high as factors of 2 and more above currently achievable levels.

d) New correlation parameters for organizing, verifying and interpreting experimental and computational results for shrouded and unshrouded propellers.

References

[1] Igar, O., "Shrouds for Aerogenerators," *AIAA Journal*, Oct. 1976, pp. 1481–83.

[2] Igar, O., "Research and Development for Shrouded Wind Turbines," *Energy Conservation and Management*, Vol. 21, Pergamon Press, New York, 1981, pp. 13–48.

[3] Riegler, G., "Principles of Energy Extraction from a Free Stream by Means of Wind Turbines," *Wind Engineering*, Vol. 7, Feb. 1983, pp. 115–126.

[4] Hansen, M. O. L., Sorensen, N. N., and Flay, R. G. J., "Effect of Placing a Diffuser Around a Wind Turbine," *Wind Engineering*, Vol. 3, No. 4, 2000, pp. 207–213. doi:10.1002/we.37

[5] Lilley, G. M., and Rainbird, W. J., "A Preliminary Report on the Design and Performance of a Ducted Windmill," College of Aeronautics, Rept. 102, Cranfield, England, 1956.

[6] Bet, F., and Grassmann, H., "Upgrading Conventional Wind Turbines," *Renewable Energy*, Vol. 28, No. 1, 2003, pp. 71–78. doi:10.1016/S0960-1481(01)00187-2

[7] Grassmann, H., Bet, F., Cabras, G., Cobia, D., and Del pap, C., "A Partially Static Turbine—First Experimental Results," *Renewable Energy*, Vol. 29, No. 4, 2003, pp. 1779–1785.

[8] Kirke, B., "Developments in Ducted Water Current Turbines," www.cyberiad.net, University of South Australia, 2005.

[9] McCormick, B. W., Jr., *Aerodynamics of V/STOL Flight*, Dover, Minneola, NY, 1999.

[10] von Kármán, T., "Theoretical Remarks on Thrust Augmentation," *Reissner Anniversary Volume, Contributions to Applied Mechanics*, edited by J. W. Edwards, Univ. Of Michigan Press, Ann Arbor, MI, 1949.

[11] Heiser, W. H., "Thrust Augmentation," American Society of Mechanical Engineers Paper 66-GT-116, 1966.

[12] Presz, W., Jr., Reynolds, G., and Hunter, C., "Thrust Augmentation with Mixer/Ejector Systems," AIAA Paper 2002-0230, 2002.

[13] Presz, W., Jr., and Werle, M., "Multi-Stage Mixer Ejector Systems," AIAA Paper 2002-4064, 2002.

[14] Quinn, B., "Compact Ejector Thrust Augmentation," *Journal of Aircraft*, Vol. 10, No. 8, Aug. 1973, pp. 481–486. doi:10.2514/3.60251

[15] Kentfield, J. A. C., "The Prediction of the Performance of Low Pressure-Ratio Thrust-Augmenter Ejectors," AIAA Paper 78-145, 1978.

[16] Porter, J. l., and Squyers, R. A., "An Overview of Ejector Theory," AIAA Paper 81-1678, 1981.

[17] Werle, M. J., and Presz, W., Jr., "Ducted Wind/Water Turbines and Propellers Revisited," *Journal of Propulsion and Power*, Vol. 24, No. 5, Sept.–Oct. 2008, pp. 1146–1150. doi:10.2514/1.37134

[18] Hansen, M. O. L., *Aerodynamics of Wind Turbines*, Earthscan, Sterling, VA, 2000.

[19] Gashe, R., and Twele, J., *Wind Power Plants*, Solarpraxis AG, Berlin, Germany, 2002.

[20] Werle, M. J., and Presz, W, Jr., "New Developments in Shrouds and Augmenters for Subsonic Propulsion Systems," AIAA Paper 2008-4962, 2008.

[21] Van Manen, J. D., and Superine, A., "The Action of Screw Propellers in Nozzles," *International Shipbuilding Progress*, Vol. 6, No. 55, March 1959, pp. 95–113.

[22] Bulten, N., and van Esch, B., "Review of Thrust Prediction Method Based on Momentum Balance for Ducted Propellers and Waterjets," *Proceedings of the 2005 ASME Fluids Engineering Division Meeting*, American Society of Mechanical Engineers, Fairfield, NJ, 2005.

[23] Weissinger, v. J., "Einige Ergebnisse aus der Theoriedes Ring Fluegels in Inkompressibler Stromung," reprinted from *Advances in Aeronautical Sciences*, Vol. 2, Pergamon Press, New York, 1959.

[24] Marc de Piolenc, F., and Wright, G., *Ducted Fan Design*, Vol I, Millenial Year edition, Mass Flow Publishing, West Covina, CA, 2001.

[25] Department of Transportation, Airworthiness Standards; Propellers, Federal Aviation Regulation Pt. 35, Federal Aviation Administration, Aug. 1974.

[26] Mattingly, J., Heiser, W., and Daley, D., *Aircraft Engine Designs*, 2nd ed., AIAA Educational Series, AIAA, Reston, VA, 2002.

A. Prasad
Associate Editor